UCRL-JC-132746
PREPRINT

# An MPP Hydrocode to Study Laser-Plasma Interactions

C. H. Still, R. L. Berger, A. B. Langdon, E. A. Williams,
L. J. Suter, S. H. Langer

This paper was prepared for submittal to the
1998 Nuclear Explosives Development Conference
Las Vegas, NV
October 25-30, 1998

**October 1, 1998**

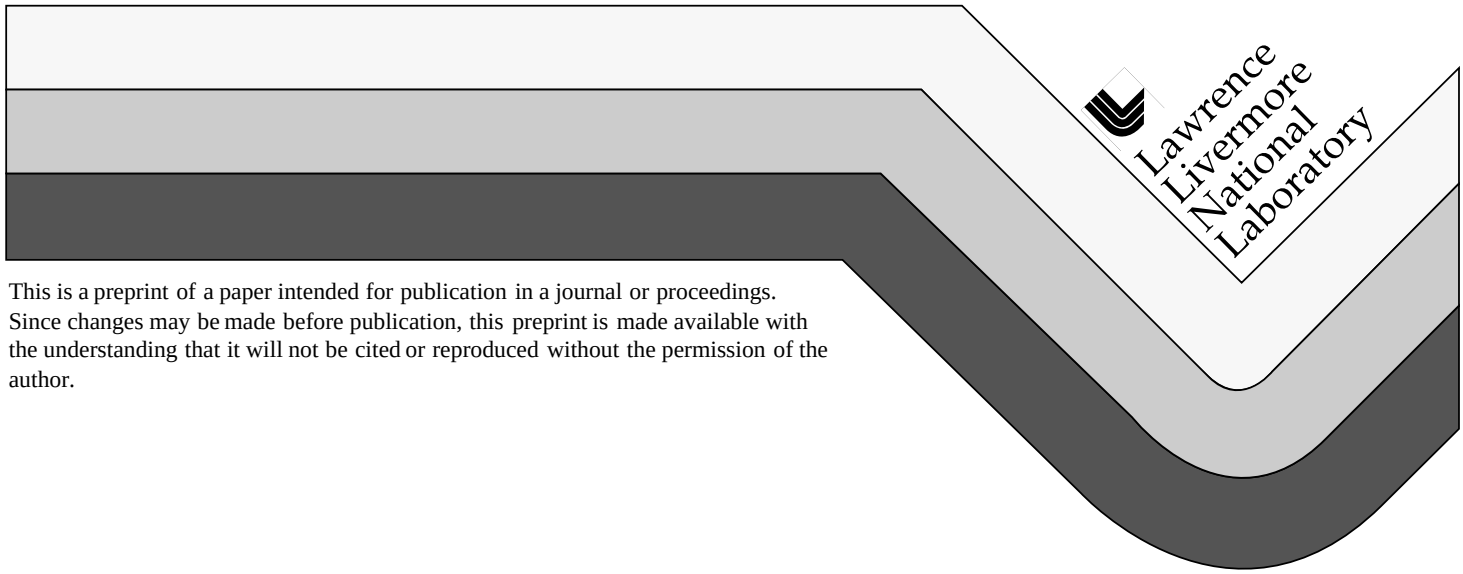

# An MPP hydrocode to study laser-plasma interactions

**C. H. Still, R. L. Berger, A. B. Langdon,
E. A. Williams, L. J. Suter, and S. H. Langer
Lawrence Livermore National Laboratory**

*Because of the increased size and power inherent in a laser-AGEX on NIF, laser-plasma interactions (LPI) observed in NOVA AGEX play an increasingly important role. The process by which filamentation and stimulated backscatter grow is complex. Furthermore, there is a competition among the instabilities so that lessening one can increase another. Therefore, simulating them is an integral part to successful experiments on NIF. In this paper, we present a massively parallel hydrocode to simulate laser-plasma interactions in NIF-relevant AGEX regimes. (U)*

**Keywords:** hydrodynamics, plasma physics, filamentation, MPP

## Introduction

In an era without underground testing, the Stockpile Stewardship Program must rely increasingly upon both above-ground experiments (AGEX) and computer simulations. This reliance has manifested itself in the funding of large projects such as the National Ignition Facility (NIF) and the Accelerated Strategic Computing Initiative (ASCI). While ASCI provides the funding to accelerate development of the advanced codes needed to calculate weapons simulations, NIF will provide AGEX data which can be used both to further understanding of weapons effects and to validate the ASCI codes.

Already there have been a number of laser-AGEX performed on NOVA, and as the physical size of the plasma in a hohlraum becomes larger or as the drive increases to obtain higher radiation temperatures, the effects of laser-plasma interactions (LPI) become more important. The primary laser-plasma instabilities are filamentation and stimulated backscatter. When a laser passes through a plasma, the ponderomotive light force will expel plasma creating local density depressions, and thereby increasing the local refractive index. The increased refraction concentrates the light into a smaller volume, thus, increasing the local laser intensity. If the local energy intensity exceeds a threshold, the self-focusing becomes unstable and filamentation results. In addition, a density fluctuation can reflect a portion of the laser light via Thomson scattering. When that backscattered light beats with the incoming wave, it can stimulate an instability. If the density fluctuation is an ion acoustic wave, the instability is stimulated Brillouin scattering (SBS). If instead it is a Langmuir wave, then stimulated Raman scattering (SRS) results. The growth rate for SBS is larger than for filamentation, but the growth rate for SRS is even larger, by almost an order of magnitude.

Each of these instabilities significantly affects the amount of energy delivered at the destination, the spectrum of that energy, and the location of delivery. Spatial beam smoothing by random phase plates (RPP) or kineform phase plates (KPP), temporal beam smoothing by spectral dispersion (SSD), or polarization smoothing (PS) can reduce the severity of these instabilities, but the amount of smoothing needed depends on the plasma conditions. Higher radiation temperatures rely on higher intensities, and higher intensities increase instability growth rates. For a fixed growth rate, longer path lengths lead to more severe instabilities once the threshold is exceeded.

Understanding plasma effects, from the simpler phenomenon of beam deflection to much more complicated issues such as the interplay among filamentation (self-focusing instability) and stimulated Brillouin and Raman backscattering (SBS and SRS), will be essential in order to design

some stockpile-relevant AGEX experiments on NIF. To this end, we are striving to develop a predictive capability for LPI.

Over the past several years, one of the main tools for studying laser-plasma interactions has been the (serial) wave-hydrocode F3D. It couples a paraxial wave solver to an Eulerian hydrodynamics package and includes models for various NOVA beam configurations, and physical processes such as SBS and SRS. Simulations done with F3D routinely use 2 GB of memory and can run for hundreds of hours for a plasma volume that is much smaller than a single NOVA beam (100 μm x 100 μm x 1 mm for the F3D simulations compared to 500 μm x 500 μm x 1 mm). A NIF beam is significantly larger than a NOVA beam. The increased scale found in a NIF beam provides ample gain length over which laser-plasma instabilities can grow, much larger path lengths than are present in NOVA experiments. For this reason, the need to model the instabilities and perform numerical experiments becomes essential, and these calculations are not tractable without a massively parallel processor (MPP). To overcome this limitation, we have begun development of a parallel F3D code (pF3d).

At present, pF3d operates as a domain-decomposed, distributed-memory MPP application on a regular 3D Cartesian grid. The code includes a (nonlinear) Eulerian hydrodynamics package (with a linearized model for nonlocal electron heat conduction) coupled to a paraxial wave solver (the equation is enveloped in time and in the laser-propagation direction). Electron density perturbations that refract and focus the laser light are driven by the ponderomotive force and by the electron pressure nonuniformity caused by the absorption of the laser light. Models are included for spatial smoothing by random phase plates (RPP) and for temporal smoothing by spectral dispersion (SSD).

In this paper, we will report on the algorithms used in the pF3d code, and present results from filamentation simulations performed on the ASCI Blue TR machine at Livermore.

## Filamentation Equations

pF3d is a parallel 3-D hydrocode in Cartesian geometry designed to simulate laser-plasma interactions. At present, pF3d can simulate filamentation and plasma effects such as beam deflection. In the future, we will include models for SBS and SRS. pF3d couples a paraxial solution of the wave equation to a nonlinear Eulerian hydrodynamics package and includes models for laser beams with KPP, RPP and SSD. For a filamentation simulation, the light propagates across the entire mesh during each time step, and the hydrodynamics then has control of the time step size ($\Delta t$) based on satisfying a Courant condition. Thus, during each time cycle, the light is advanced across the computational mesh, and then the hydrodynamics equations are advanced a time step. Inclusion of the SBS and SRS models necessitate resolving the light transit and the instability growth time so that the algorithm changes to propagate the light one plane axially per time step. The simulation box is aligned along the propagating laser beam to model experiments done in gas bags or hohlraums (see Figure 1); laser-AGEX are generally done inside hohlraums.

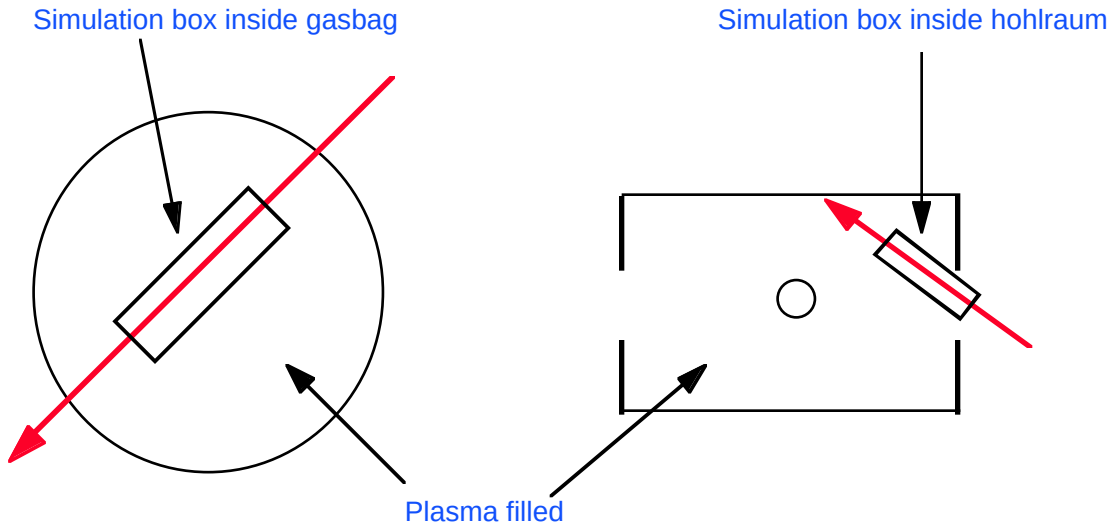


**Figure 1. The simulation box sits inside a gas bag or a hohlraum**

Because in filamentation the frequency $\omega_0$ and wavenumber $k_0$ of the incident light are only slightly perturbed, an envelope approximation in time and space is reasonable. The resulting paraxial wave equation is

$$\left(\frac{\partial}{\partial t}+v_g\frac{\partial}{\partial z}-\frac{ic^2}{2\omega_0}D_\perp^2+\frac{1}{2}\frac{dv_g}{dz}+\nu\right)E=-\frac{4\pi e^2 i}{2\omega_0 m_e}\delta n_e E \tag{1}$$

where $D_\perp^2=\dfrac{2k_0\nabla_\perp^2}{k_0+\sqrt{k_0^2+\nabla_\perp^2}}$ is the modified diffraction operator due to Feit and Fleck (1988), $v_g=\dfrac{c^2k_0}{\omega_0}$ is the group velocity of the incident light, $\nu$ is the collisional amplitude-absorption rate, $\delta n_e$ is the perturbation of the electron number density and $E$ is the (complex) electric field. Solution of the paraxial equation (1) is achieved by splitting the equation into three parts and solving each separately. The three resulting equations represent the physical processes of refraction, diffraction and propagation, and absorption, respectively:

$$v_g\frac{\partial}{\partial z}E=-\frac{4\pi e^2 i}{2\omega_0 m_e}\delta n_e E \tag{2}$$

$$\left(v_g\frac{\partial}{\partial z}-\frac{ic^2}{2\omega_0}D_\perp^2\right)E=0 \tag{3}$$

and

$$\left(v_g\frac{\partial}{\partial z}+\frac{1}{2}\frac{dv_g}{dz}+\nu\right)E=0. \tag{4}$$

The light advance is handled by a splitting technique: the refraction equation (2) is advanced by half a cell $\Delta z/2$, then the diffraction equation (3) is advanced a full step $\Delta z$, and the refraction equation

(2) is advanced the final Δz/2. Finally, the absorption (4) is computed for the entire time step Δt. The refraction step is done using finite differences, and the diffraction and absorption calculations are done using spectral methods (and hence involve a series of 2-D FFTs).

The Eulerian hydrodynamics equations are as follows. The continuity equation is

$$\frac{\partial}{\partial t}\rho + \nabla \bullet (\mathbf{v}\rho) = 0 \tag{5}$$

where $\rho = \frac{A}{Z}\frac{n_e}{n_c} = A\frac{n_i}{n_c}$ is the mass density, and **v** is the fluid velocity. Note that we assume quasi-neutrality of the plasma $n_e = Zn_i$. The momentum equation is

$$\frac{\partial}{\partial t}S_j + \nabla \bullet (\mathbf{v}S_j) + \nabla \bullet \mathbf{Q}_j + \frac{\partial}{\partial x_j}P + \frac{\partial}{\partial x_j}P_e + \rho\frac{\partial}{\partial x_j}\varphi = 0 \tag{6}$$

where $\mathbf{S} = \rho\mathbf{v}$ is the momentum density, P is the ion pressure, $P_e$ is the electron pressure, φ is the ponderomotive force due to the light, and **Q** is an artificial viscosity. The ion energy equation is written in a form where ion pressure is the fundamental quantity [using the ideal gas equation of state, $\frac{3}{2}P = \frac{3}{2}nT = \rho\varepsilon$]

$$\frac{3}{2}\left(\frac{\partial}{\partial t}P + \nabla \bullet (\mathbf{v}P)\right) + P\nabla \bullet \mathbf{v} + \mathbf{Q} : \nabla\mathbf{v} = 0. \tag{7}$$

Finally, the electron energy equation is written in the linearized form

$$\frac{\partial}{\partial t}\delta T_e + \delta T_e \nabla \bullet \mathbf{v} = -\nabla \bullet \delta\mathbf{q}_e + \delta H_e \tag{8}$$

where $\delta\mathbf{q}_e$ represents nonlocal thermal conduction and $H_e$ is a heat source from inverse Bremsstrahlung absorption. The hydrodynamics update is done by operator splitting the equations and applying finite difference solutions, except for the calculation of the nonlocal electron heat conduction which is done in *k*-space. The advection terms are handled by a 2nd order van Leer scheme. The additional terms of the momentum and energy equations are handled individually (see Still et al, 1996). The boundary conditions are periodic in the directions transverse to the propagating laser. For the case that the simulation volume is smaller than a laser beam, this is consistent with the idea that surrounding the simulation box in the transverse directions are other equivalent pieces of the beam. In the case that the simulation box is larger than the beam, the simulation size should be chosen to make the distance from the beam to the (transverse) boundaries as large as possible. Linearizing the electron energy equation is justified since the electron temperature perturbations tend to be small, but otherwise, the nonlinear terms are needed because of the strong ponderomotive drive from lasers with high intensity (typically found in laser-AGEX such as high temperature hohlraums).

**MPP Performance**

The computational mesh is decomposed into rectangular domains, partitioning over the two directions transverse to laser propagation, but not over the axial direction. The reason for not dividing the problem axially is that for the filamentation calculation the assumption of light transit in a single time step serializes the propagation calculation. In the future, the addition of SBS and SRS models will require changing the propagation algorithm, and axial domain decomposition will be included. The electric field does not require any guard cells, but there is one layer of guard cells for hydrodynamic quantities.

pF3d uses the MPI form of message passing. The majority of the communications cost occurs in updating the guard cells within the hydrodynamic advance, and within the FFT used during the light advance. Message passing time used during diagnostics, plotting, and dumping restart files are minimal by comparison. The hydrodynamic guard cell updates are performed as shift operations within the context of individual row and column communicators (see Figure 2). This paradigm performs well, as shown below.

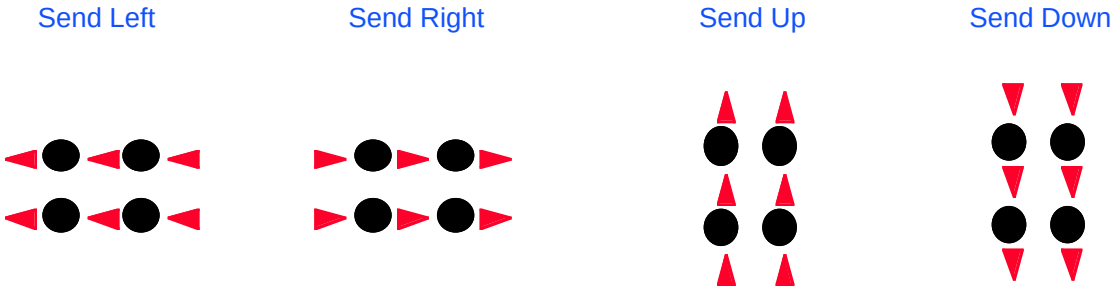


**Figure 2. Communication pattern for hydrodynamics guard cell updates**

The number of messages to update a hydrodynamics quantity is O(2P+2Q) for a PxQ processor grid. The length of the messages depends on which hydrodynamics quantity is being updated.

The parallel 2-D FFT routine uses an index operation for its communication. Each processor gathers the columns of the data to be transformed from within its processor column, applies a serial 1-D FFT and scatters the data back out to the processor column. Then, the processor transposes its local copy of the data and repeats the previous operation, but for rows of data within a processor row. After the scatter back throughout the row, the data is locally transposed once more to produce the local image in frequency space. The inverse parallel FFT is done by inverting the algorithm. This implementation of the parallel FFT does not minimize the communication cost, but it does attempt to maximize cache efficiency of the 1-D FFTs.

In performing scalability testing on the IBM SP/2 with the multiple user space communication capable hardware (MUSPPA), we find the code performs well . The problem size was scaled with the number of processors to ascertain the effect of the increased communications found in larger problems. Figure 3 shows curves of run time versus total number of processors for the cases where either one processor per node was used, or where all four processors per node were used, and for both the faster user-space communications paradigm or the slower internet-protocol. In the case of single processor per node use with the faster communications mode, scalability was quite good, less than 5% degradation. For the multiprocessor per node case with user-space communications, degradation approached 15% . For the internet-protocol communications cases, the degradation is 12% for single processor runs and 36% for the multiprocessor runs.

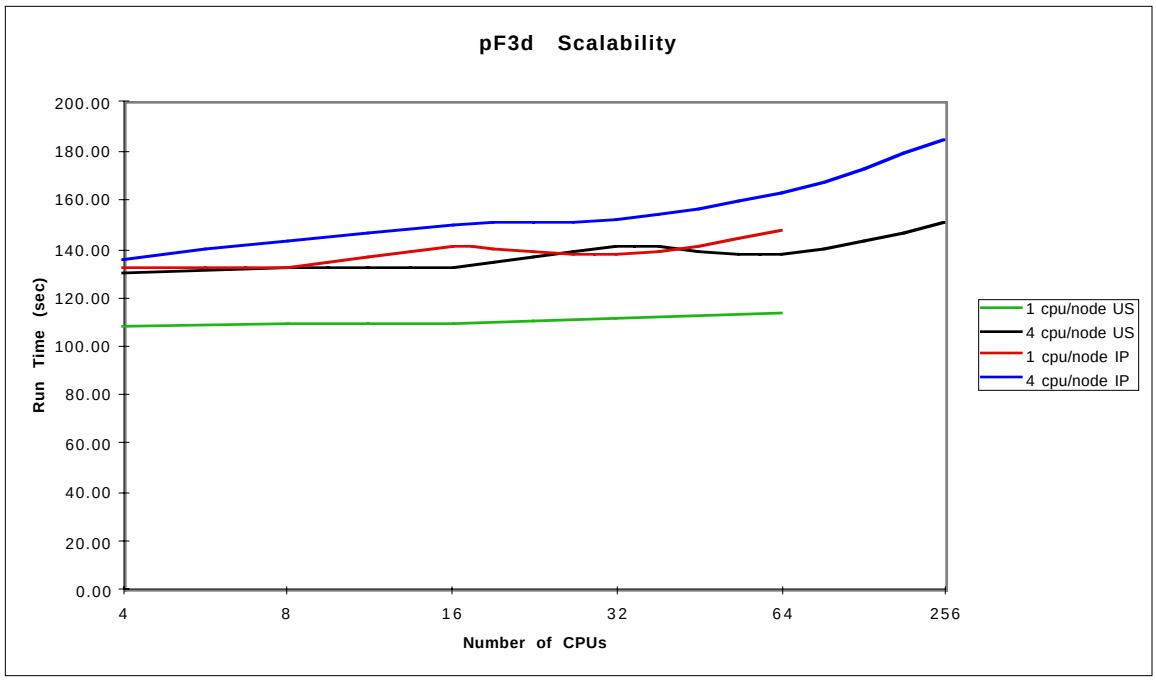


**Figure 3. Scalability of the pF3d code on the IBM SP/2**

Developing a parallel hydrocode, regardless of efficiency, would have been insufficient without the accompanying improvements in MPP computers. In order to simulate the plasma volume of an entire NIF beam (700 μm x 700 μm x 2.5 mm), computations must be carried out on a 900 μm x 900 μm x 2.5 mm grid with 5.9 billion zones (total problem size for filamentation is 328 GB of memory). Currently, we have done filamentation simulations with the first dimension reduced by a factor of 16 because of memory limitations; the reduced problem has 367 million zones and can complete 1 ps of simulation in about an hour on 64 nodes of the ASCI Blue Pacific machine at LLNL. In the graph below (Figure 4), we show how the run times for a 250 ps filamentation simulation and a 50 ps LPI simulation including SBS physics on the 5.9 billion zone problem would have changed over the past few years, if the calculation could have been done. The extrapolations in previous years are made by scaling the performance of the serial F3D code, or the pF3d code from simulations on other sized problems. The extrapolations in future years are made by scaling current performance by reasonable expectations (and not theoretical peak performance) of follow-on ASCI machines.

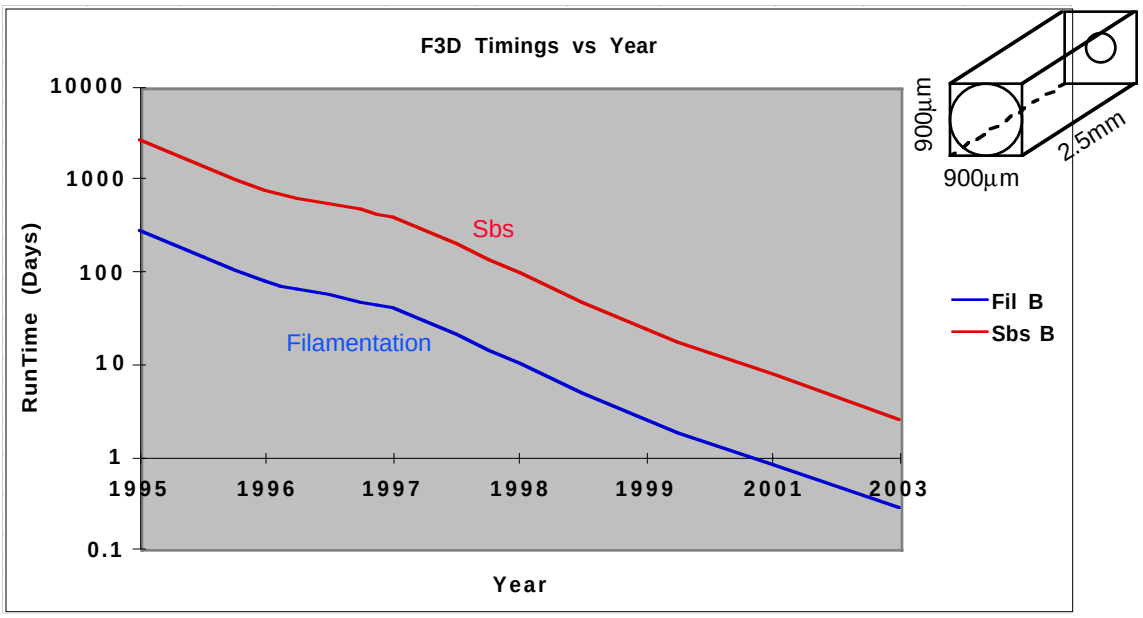


**Figure 4. pF3d extends simulation capabilities to plasma volumes approaching a NIF beam**

## NIF-Relevant Simulations

The simplest laser-plasma interaction relevant to NIF experiments is beam deflection. A flowing plasma will develop a density gradient in the direction of the flow. Laser energy will refract off of the density gradient deflecting the path of the beam in the direction of the flow. This phenomenon has been seen experimentally, and can be modeled in simulations (see Young et al, 1998). Beam deflection is important in laser-AGEX, particularly near the laser entrance hole where the plasma flow is strongest, because it can cause the laser to miss the intended impact point, thereby depositing laser energy at unintended locations within the hohlraum. We will not address beam deflection here.

Stimulated Brillouin backscatter (SBS) and stimulated Raman backscatter (SRS) act to reduce the amount of energy in the laser. Whereas filamentation is a result of a self-focusing instability, stimulated backscatter results from a resonant interaction of the incident light wave with either an ion acoustic wave (SBS) or a Langmuir wave (SRS). Both SBS and SRS are important, and in particular, SBS has been shown experimentally to be important in the region of gold blowoff near the hohlraum wall. These instabilities are not yet included in pF3d, so we will instead focus on filamentation.

Rather than model filamentation effects in any specific AGEX, we choose to study a generic high temperature hohlraum (HTH) design that is NIF-relevant. Using a 3/4-scale NOVA hohlraum and *f*/8 RPP beams with NIF power, we model the interaction of one of the RPP beams with the gold blowoff from the hohlraum wall. The average initial laser intensity at the focus of the *f*/8 lens is $10^{16}$ W/cm$^2$ with a wavelength of $\lambda_0$ = 351 nm, and has a 10 ps rise time. The plasma size is taken to be 112 µm x 112 µm x 181 µm, starting 231 µm inside the laser entrance hole (LEH) where the laser is focused. The beam is shaped so that it fills roughly 75% of the box in the transverse directions. Using plasma parameters from a LASNEX simulation at 500 ps into the laser pulse, we take the initial density $n_e/n_c$ to be a ramp from 2% to 20% over the first 80 µm and

then constant at 20% for the rest of the plasma length. The electron and ion temperatures are roughly uniform over the region, so we take $T_e$ = 20 keV and $T_i$ = 10 keV.

The figure below (Figure 5) shows an axial slice through the center of the beam and the corresponding slice through the plasma. These images are taken after 38 ps of simulation time. During this time, the beam has focused into hot spots with a peak energy intensity of 3 x $10^{17}$ W/cm$^2$. The larger of the hotspots has dug a channel (the density perturbation is approximately 30% from the walls of the channel to the center of the channel). As the channel grows, it contributes to the self-focusing of the beam: the light refracts off the walls of the channel into the density trough.

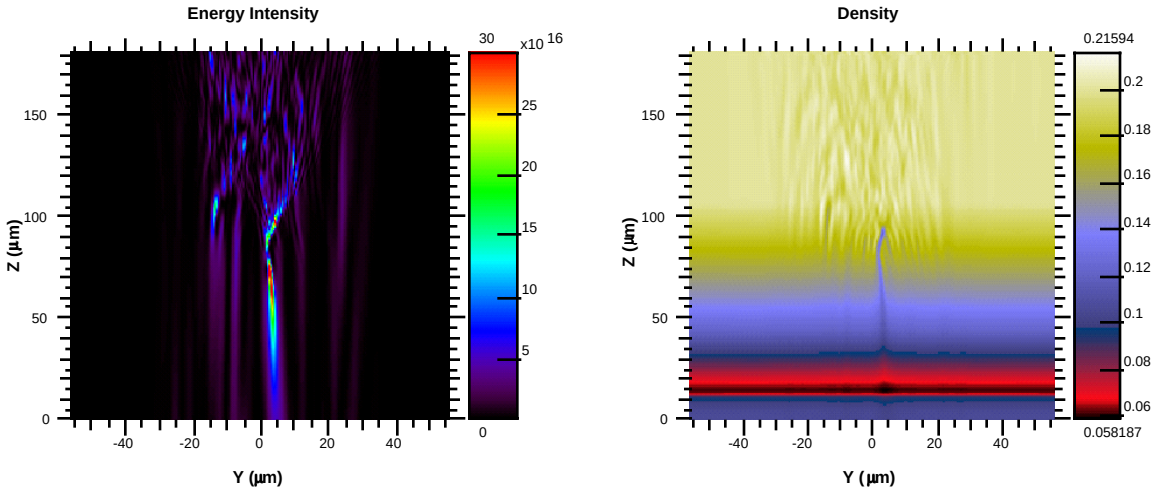


**Figure 5. Slice through the center of the box showing the energy intensity of the beam and the channel developing in the plasma**

As shown in the previous figure (Figure 5), acoustic waves form at the front of the propagating beam. These waves are driven by the ponderomotive force and travel away radially at the ion acoustic velocity. They induce a temporal smoothing of the laser beam by the plasma by disrupting density channels as the channels begin to form. On the left of the next figure (Figure 6) we show a slice through the density halfway down the axis of propagation taken at the same time (+38 ps). Note the visible rings of the ion acoustic waves emanating from the center of the density channel. On the right half of the figure is the density at the transmission plane (near the hohlraum wall). The superposition of the acoustic waves prevents the light from focusing as strongly and the density depressions are less than those at the mid-plane. Specifically, the lowest density on the transmission plane is just under 0.18 $n_c$ representing a 10% perturbation from the initial state (0.2 $n_c$); however, the mid-plane shows density perturbations of up to 30% from its initial state (a low of 0.13 $n_c$ out of approximately 0.19 $n_c$) indicative of strong self-focussing.

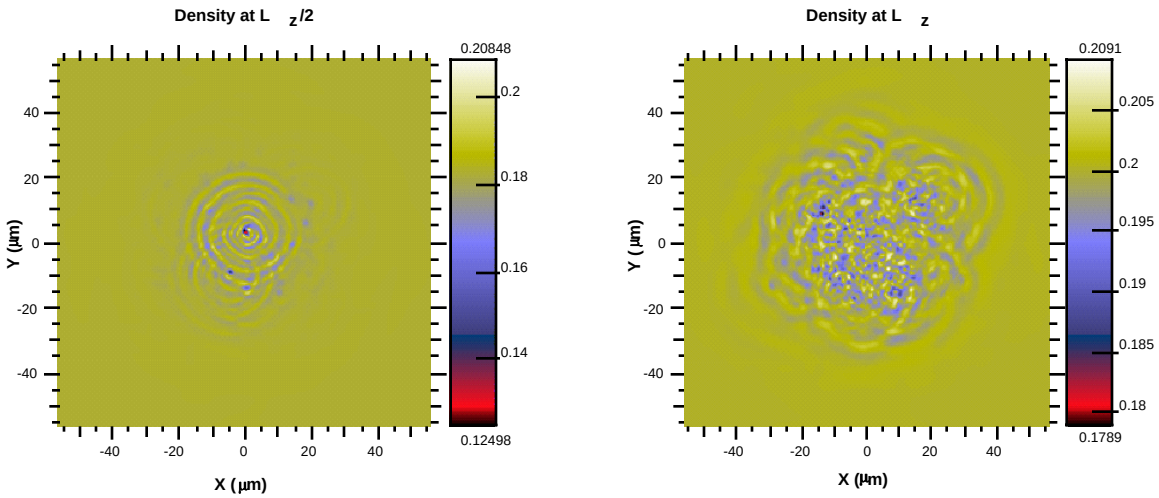


**Figure 6. Transverse slices of the density at halfway through the plasma volume and at the end of the box**

With the plasma-induced smoothing and the shorter path length of a 3/4-scale NOVA hohlraum, filamentation is expected to be low. In the figure below (Figure 7), we compare the energy intensity at the incident and transmission planes. Note that the peak intensities are comparable around 6 x $10^{16}$ W/cm$^2$), but that the transmitted light exhibits much finer scale structure. The fine scale structure is caused by breakup of the larger hotspots due to filamentation. Since the path length is relatively short, the beam has not spread appreciably. Also important to note is the fact that almost all of the transmitted energy remains inside the same areal spot found on the incident plane. The fine scale structure shows that energy is being transferred to higher wavenumbers, but the path length is short enough that the energy is not being sprayed out to large angles.

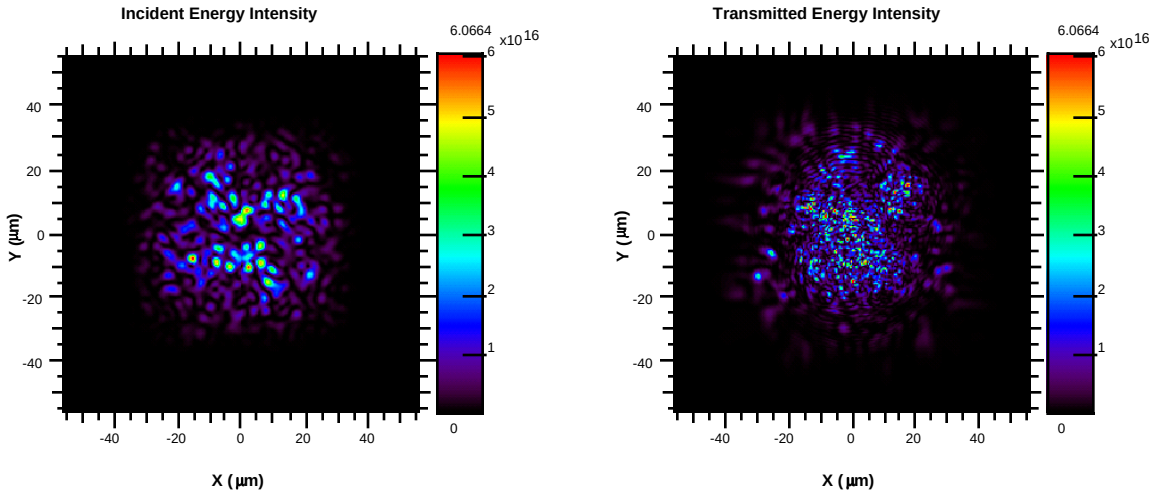


**Figure 7. Comparison of the energy intensity of the incident and transmitted light**

For this example, filamentation is fairly benign, and the laser energy remains collimated. If the hohlraum was larger, leading to a longer laser path and a possibly much lower electron temperature, beam spreading would likely be much higher, and filamentation more severe. Even

though filamentation is low, SBS could be expected to be more important, emphasizing the need for incorporating the SBS and SRS models into pF3d.

## Conclusions and Future Work

In the larger scale and higher power experiments to be fielded on NIF, laser-plasma instabilities will play a very important role. Increased path lengths give instabilities with even moderate gain rates much more opportunity to grow, and the severity increases with laser intensity. The complexity of the interaction and competition among filamentation, stimulated Brillouin backscatter and stimulated Raman backscatter coupled with the critical role they play make LPI modeling an essential element in fielding successful experiments on NIF. However, the same larger scales that make the LPI effects more dramatic also serve to make their simulation much more difficult. A serial code, or even an SMP code is not sufficient. Thus, we have begun developing a massively parallel LPI hydrocode, pF3d.

Using pF3d, we can model filamentation and beam deflection in NIF-relevant plasma volumes and include the simulation results in the AGEX design process. SBS and SRS models are included in the serial code F3D and currently under development for the MPP code, and will be included in future AGEX LPI modeling efforts.

Ray-tracing-based models of laser beams can accurately transport the laser energy, but cannot resolve the wave interactions necessary to model LPI. Wave-based calculations can resolve LPI and accurately transport the laser energy, but the size and runtime associated with a single-beam simulation suggest that an integrated hohlraum calculation including wave-based models is intractable in the near future. By studying laser-plasma interactions, we expect to develop reduced descriptions of physics and thereby improve the ray-based models. In the meantime, we will continue striving to develop a predictive capability for LPI.

## Acknowledgments

This work was performed under the auspices of the United States Department of Energy by the Lawrence Livermore National Laboratory under contract number W-7405-ENG-48.

## References

Berger, R. L., Lasinski, B. F., Kaiser, T. B., Williams, E. A., Langdon, A. B., and Cohen, B. I., "Theory and three-dimensional simulation of light filamentation in laser-produced plasma," *Phys. Fluids B*, **5**, 7 (1993).

Berger, R. L., Still, C. H., Williams, E. A., and Langdon, A. B., "On the dominant and subdominant behavior of stimulated Raman and Brillouin scattering driven by nonuniform laser beams," submitted to *Phys. of Plasmas* (1998).

Feit, M. D. and Fleck, Jr., J. A., *J. Opt. Soc. Am. B*, **5**, 633 (1988).

Still, C. H., Berger, R. L., Langdon, A. B., and Williams, E. A., "Three-dimensional nonlinear hydrodynamics code to study laser-plasma interactions," *ICF Quarterly Report*, Lawrence Livermore National Laboratory, Livermore, CA, UCRL-LR-105821-96-4 (1996).

Young, P. E., Still, C. H., Hinkel, D. E. Kruer, W. L., Williams, E. A., Berger, R. L., and Estabrook, K. G., "Observations of laser-beam bending due to transverse plasma flow," *Phys. Rev. Lett.*, **81**, 7 (1998).